

A HEAT TRANSFER MODEL FOR FIREFIGHTERS' PROTECTIVE CLOTHING

by

**William E. Mell and J. Randall Lawson
Building and Fire Research Laboratory
National Institute of Standards and Technology
Gaithersburg, MD 20899 USA**

Reprinted from Fire Technology, Vol. 26, No. 1, 1st Quarter, February 2000.

NOTE: This paper is a contribution of the National Institute of Standards and Technology and is not subject to copyright.

NIST

**National Institute of Standards and Technology
Technology Administration, U.S. Department of Commerce**

A Heat Transfer Model for Firefighters' Protective Clothing

William E. Mell and J. Randall Lawson

Abstract

An accurate and flexible model of heat transfer through firefighter protective clothing has many uses, including investigating the degree of protection, in terms of burn injury and heat stress, of a particular fabric assembly and analyzing cheaply and quickly the expected performance of new or candidate fabric designs or fabric combinations.

This paper presents the first stage in developing a heat transfer model for firefighters' protective clothing. The protective fabrics are assumed to be dry, which means no moisture from perspiration, and the fabric temperatures considered are below the point of thermal degradation, such as melting or charring. Many firefighter burns occur even when there is no thermal degradation of their protective gear. A planar geometry of the fabric layers is assumed with one-dimensional heat transfer. The forward-reverse model is used for radiative heat transfer. The accuracy of the model is tested by comparing time-dependent temperatures from both within and on the surface of a typical fabric assembly to those obtained experimentally. Overall, the model performed well, especially inside the garment where the temperature difference between the experiment and the simulation was within 5°C. The predicted temperature on the outer shell of the garment differed most from experimental values, by as much as 24°C. This was probably due to the absence of fabric-specific optical properties, such as transmissivity and reflectivity, used for model input.

1 Introduction

The thermal performance of firefighters' protective clothing has been a point of interest and discussion for several decades. However, little detailed scientific information is available on the technical issues. Much of these discussions are based on fire service field experience, and many of these studies are difficult to reproduce. Very little has been done to develop methods for predicting the thermal performance of protective clothing throughout the range of fire environments a firefighter normally faces.

Torvi¹ provides a review of work done on heat and mass transfer models applicable to fabrics in the high heat flux range that a firefighter may experience. Most of this work dates from the 1960s² and 1970s³, when computers were significantly less advanced. The Government-Industry Research Committee on Fabric Flammability considered mainly flammable fabrics used by the ordinary consumer.^{3,4} Morse *et al.*⁵ studied heat transfer and burn injury risk from exposure to JP-4 fuel fires. Only three protective clothing materials were examined for use in U.S. Air Force flight suits. Also, some model properties were determined by fit-

Key Words: heat transfer; computer modeling; fire; firefighter; firefighter safety; protective clothing; thermal insulation; turnout coats

ting the model results to experimental data. Stoll and colleagues used a combination of analytical and experimental techniques to measure the thermal response of single fabric layers over skin.⁶⁻⁸ They developed diagnostics to rate the protection offered by a fabric with known properties. Their work eventually led to the thermal protective performance (TPP) test.⁹ Recently, Bamford and Boydell¹⁰ developed a finite-difference-based burn injury evaluation code, and Torvi¹ developed a finite element code to simulate the TPP test.

NFPA 1971, *Protective Ensemble for Structural Fire Fighting*,¹¹ has two thermal performance tests: a fabric flammability test and the TPP test. These tests, along with the development of new fabrics with improved thermal properties, have led to significant changes in firefighter clothing. The fabric flammability test has resulted in the development of protective garments that resist flaming ignition. The TPP test has led to the improved performance of protective clothing under relatively short-duration, high-heat-flux conditions. This is because the TPP test was originally designed to test fabric performance under short duration, high heat flux exposures, such as flash fires and JP-4 fuel fires from deck crashes of planes on aircraft carriers. The NFPA standard TPP test method measures heat flow through the garment while exposed to a 84 kW/m² (2 cal/cm²·s) thermal environment. This level of flux is chosen to replicate a flash fire or mid-range post-flashover exposure. A single copper calorimeter measures heat transfer through a protective clothing assembly, and no data are gathered on the thermal performance of individual protective clothing components.

A minimum TPP rating of 35 is required, according to NFPA 1971. At this level of protection, a firefighter would have approximately 17.5 seconds to escape from a flashover exposure before sustaining second-degree burns. This prediction is based on the assumption that the experimental conditions in the TPP test, such as a 84 kW/m² heat flux, half convective and half radiative, and the assumptions in the burn injury model, such as a direct contact of the turnout coat with skin of certain properties, adequately represent a firefighter in a flashover. However, work by Krasny *et al.*¹² suggests that firefighters wearing TPP 35 garments are likely to receive serious burns in less than 10 seconds when exposed to flashover. Peacock *et al.*¹³ found that the TPP test was best able to predict the relative thermal protection of different turnout gear in room fires that were rapidly developing into flashover.

To date, the TPP test is the only source of data relevant to the thermal performance of protective clothing. It is relatively inexpensive, though somewhat complicated, to run and only provides the user with thermal performance of the protective garment as a whole. A more informative test method would provide thermal performance measures of the component fabrics and, therefore, heat transfer within the garment. TPP test measurements are also time-restricted because of the thermal properties of the copper calorimeter. Generally, TPP tests on thermal protective clothing have been conducted using periods of less than 1 minute.¹¹

Thus, the TPP test does not produce the detailed information necessary for evaluating the thermal performance of protective clothing over a range of conditions. This is an important issue since many firefighter burns appear to result from longer-duration, moderate-heat-flux exposures.¹⁴

Firefighters can be burned by radiant heat produced by a fire or by a combination of radiant energy exposure and localized flame contact, as replicated by the TPP test. Some injuries also occur as a result of compressing the protective garment against the skin, either by touching a hot object or by placing tension on the fabric until it becomes compressed against the skin. In addition, moisture in protective clothing can significantly change the garment's protective performance. As stated in NISTIR 5804, wet garments may exhibit significantly higher heat-transfer rates than dry garments.¹⁴ Burns that result from the heating and evaporation of moisture trapped in protective clothing—generally referred to as scald or steam burns—are also significant. Moisture may also help to store heat energy in protective clothing.¹⁴

The Building and Fire Research Laboratory (BFRL) at the National Institute of Standards and Technology (NIST) has been developing two tools to further the understanding and prediction of the thermal performance of firefighters' protective clothing. One tool is a laboratory test apparatus that exposes specimens of protective clothing to radiant heat from a gas-fired radiant panel and/or flames from a gas pilot line burner. The temperature can be measured by placing thermocouples on and in the fabric assembly.

This experimental test apparatus, discussed in the next section, was designed to measure the temperature distribution through layers of protective clothing over a range of conditions. It is possible to subject the protective clothing materials or specimen to various levels of incident radiant heat flux and to investigate the effects of compression and moisture.

The second tool is the subject of this paper. It is an analytical computer model that provides detailed information on heat transfer through the protective clothing assembly. Among the other models developed to date, this model is most similar to that of Bamford and Boydell.¹⁰ However, development of the model discussed here will occur in stages. The performance of the model will be tested by comparing temperature predictions to measurements from the laboratory test apparatus. Ultimately, a detailed skin model can be included if needed to provide burn injury predictions. When fully developed, this predictive model could be used as an aid in the design of candidate protective clothing systems, evaluating the performance of current protective clothing systems in various thermal environments, and as a tool to study potential issues related to the causes of firefighter burns. It could also be used as a training tool for fire service personnel.

In the next section, a brief description of the experimental test apparatus is given. The derivation of the heat transfer model is presented in the third section, followed by its numerical implementation, the thermophysical characteristics of

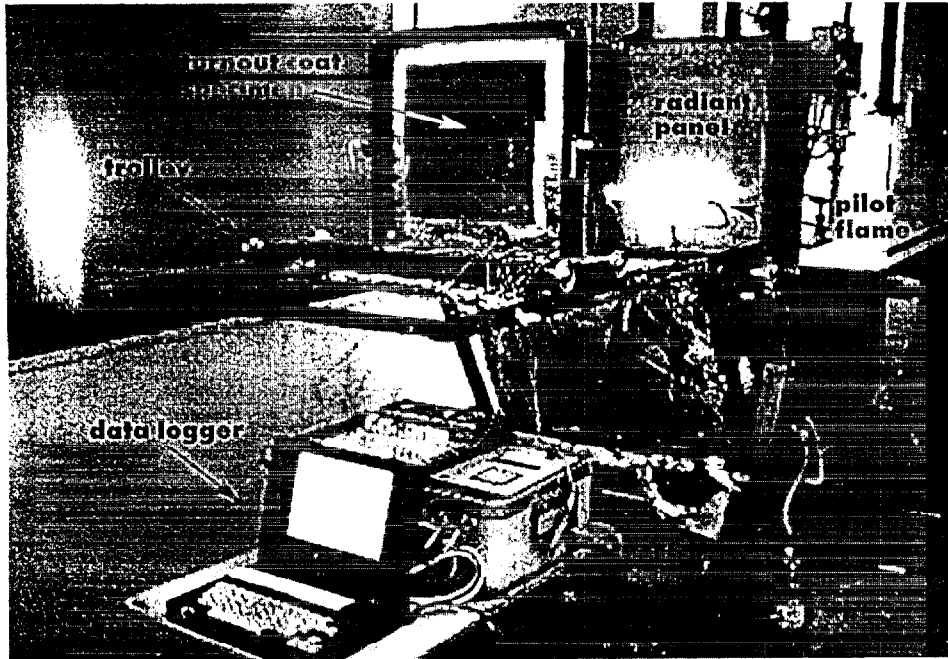


Figure 1.

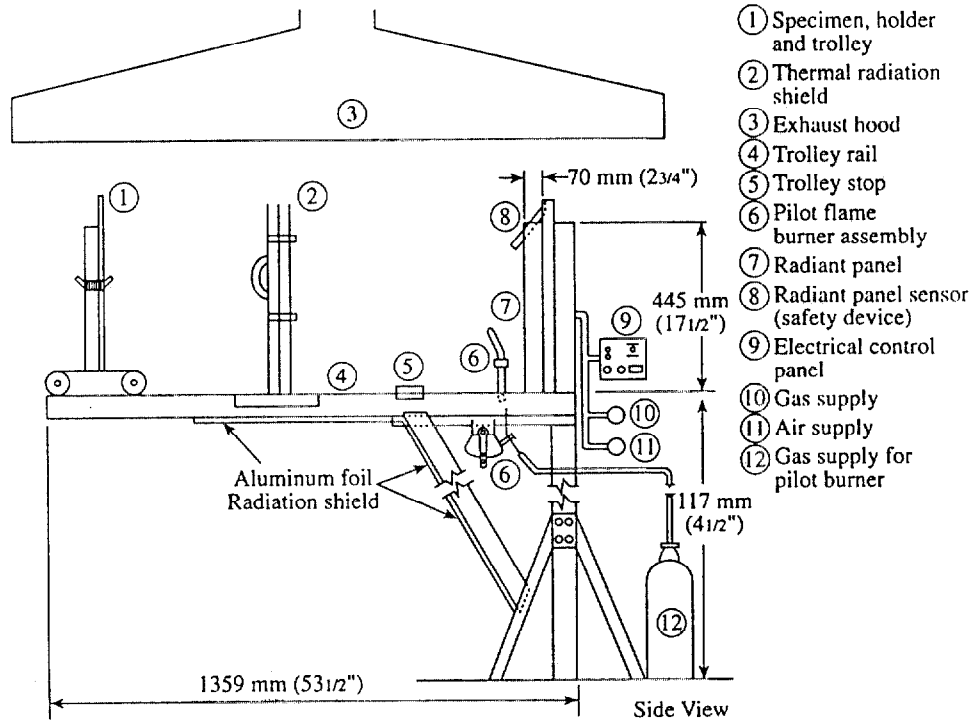


Figure 2.

the turnout coat considered here, and model predictions versus experimental results.

Experimental Test Apparatus

The test apparatus¹⁵ was designed to evaluate the thermal performance of firefighters' protective clothing over a wide range of thermal exposures. Results from the test provide a thermocouple-based time history of the temperature at

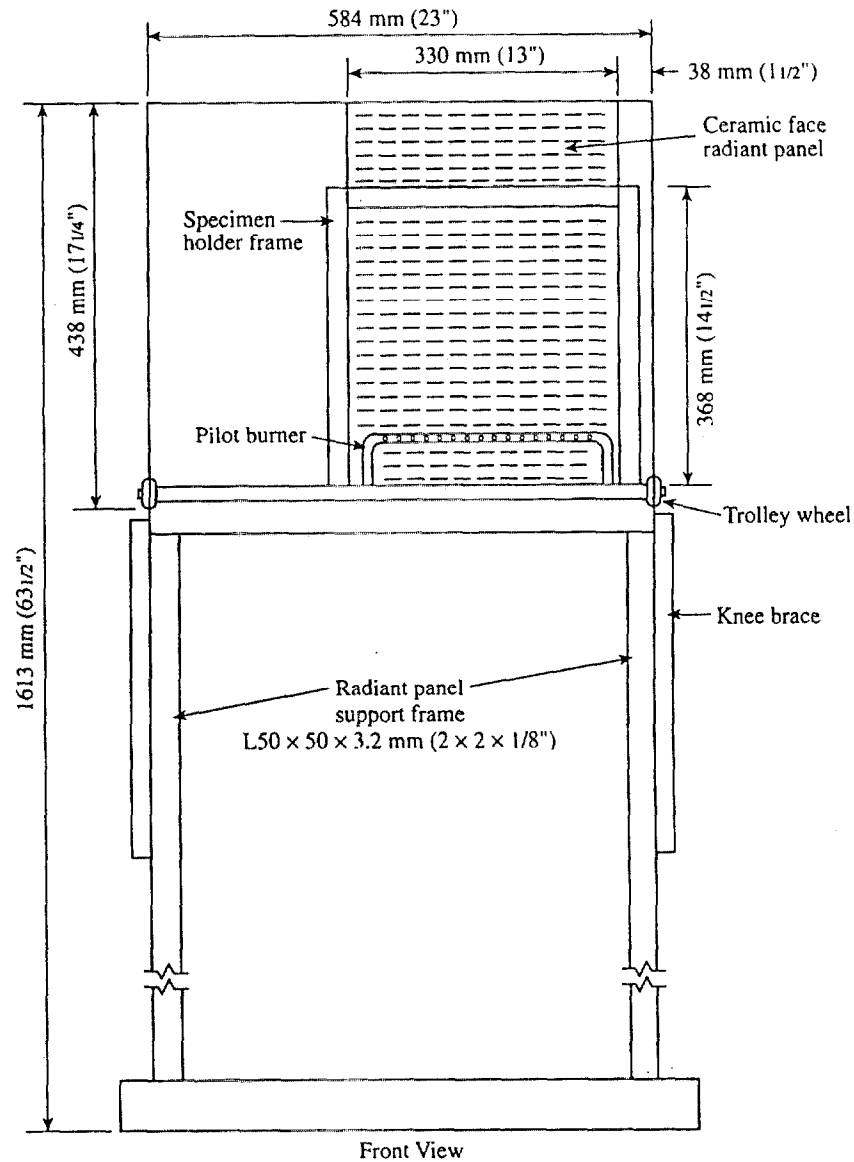
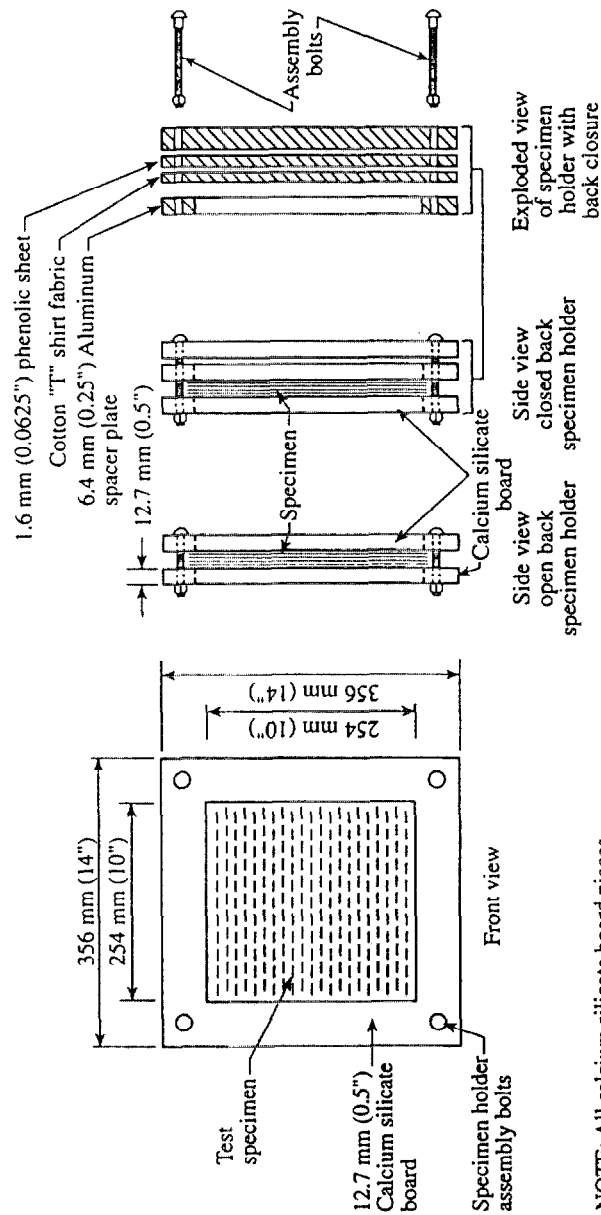


Figure 3.

NOTE: Exhaust hood located above test apparatus

fabric layer surfaces, such as the outer or inner surface of a garment assembly or between component layers. In addition, the test method may be used to measure latent heat or energy stored in the clothing assembly when it is exposed to a selected thermal environment for a specified period of time.

Figures 1 through 3 show the test apparatus and its components. The specimen holder is mounted on a trolley, which allows the specimen to be moved easily and



NOTE: All calcium silicate board pieces except the back closure are covered with 0.05 mm (0.002 in) thick aluminum foil. The back closure consisting of the phenolic sheet and calcium silicate board are covered with cotton "T" shirt fabric that is held in place on the closure's back surface with duct tape.

Figure 4.

secured at different distances from the radiant panel. In this way, the radiant flux, due to the radiant panel, incident on the outer surface of the garment specimen can range from about 1.0 kW/m² to more than 50 kW/m². The test specimen may also be subjected to a pilot flame during any part of a test to evaluate the thermal performance associated with direct flame contact. Test specimens in Figure 4 measure 305 mm by 305 mm. The specimen surface, which is exposed to test conditions, measures 255 mm by 255 mm when held in the specimen holder. (See photograph showing the test specimen prepared for test in Figure 1 and the sketch of the specimen holders in Figure 4.) This specimen size was selected to allow for the measurement of protective clothing system assemblies that may have surface features, such as trim, pads, patches, or pockets, that require evaluation. Tests may be conducted with either an open-back or closed-back configuration. We only used the open-back configuration. Figure 5 shows the basic locations for thermocouple attachment. A minimum of three thermocouples is required to measure heat flow through a garment assembly. These are Thermocouples 1, 2, and 3 in Figure 5. Thermocouple 4 is used to measure open field temperatures when a surface attachment is applied to the shell material. Protective clothing specimens may be tested dry or wet to measure the effects of moisture.

In this study, the test apparatus was used to help gauge the validity of the heat

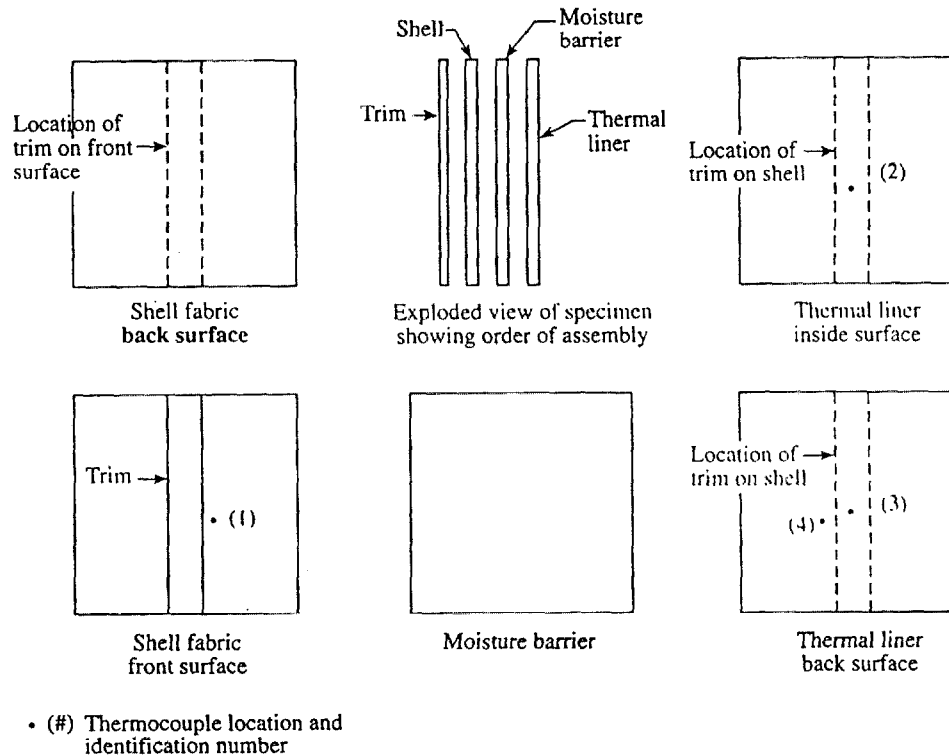


Figure 5.

transfer model developed below. Since this is the first stage in developing the model, conditions were kept simple. Thus, experimental results are for dry specimens in the open-back configuration. Only the radiant panel was used; there was no direct flame contact.

In the following section, a one-dimensional model for heat transfer in firefighter protective clothing will be developed. The assumption of one-dimensional heat transfer would not be valid if the temperature varied significantly across the face of the test specimen. However, temperatures were found to vary only by $\pm 5^\circ\text{C}$ across the central third of the specimen. Total heat flux calibrations were made before each set of runs using a water-cooled Schmidt-Boelter gauge.

For test reference purposes, the heat flux calibration point was marked on the apparatus during the runs. Calibrations were usually done several times a day as different test exposure conditions were needed. The test specimens were conditioned to equilibrium at 23°C , $\pm 3^\circ\text{C}$ and 50%, $\pm 10\%$ RH before testing. Specimens were tested within 10 minutes after they were removed from the conditioning environment.

The cotton thread used to attach the thermocouples showed no signs of thermal damage following the test, and there was no thermocouple separation from the specimen. Flame-resistant (FR) thread is used to attach thermocouples when test conditions are likely to cause visible thermal degradation to fabrics.

3 Heat Transfer Model

This work is the first step in developing a heat-transfer model for firefighter protective clothing. Heat transfer through a firefighter's clothing, ultimately reaching the skin, is largely due to radiant energy from the surroundings. This process, as opposed to direct contact with flames, is the focus of the current stage of the model. The influence of moisture is not considered, and temperatures are

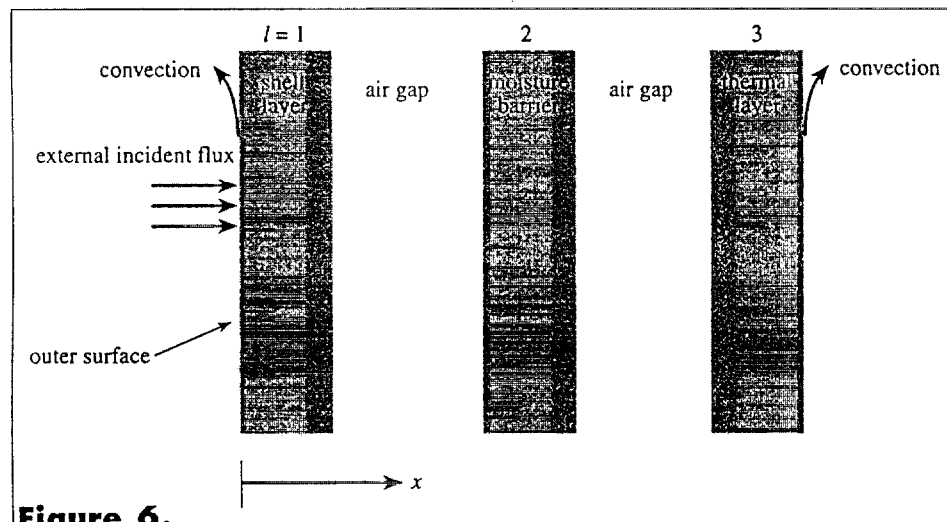


Figure 6.

assumed to be too low to melt or gasify the fabrics—that is, to thermally degrade the fabric. Many firefighter burn injuries occur even when there is little or no thermal degradation of protective gear. Hopefully, the heat transfer model and the experimental test apparatus discussed here will lead to a better understanding of why these injuries occur and how they can be prevented.

Figure 6 shows a sketch of a typical, three-layered firefighter protective clothing fabric ensemble, such as a turnout coat. This geometry is identical to the experimental test apparatus discussed in the previous section. Because it is both an appropriate first modeling step and consistent with the experimental test apparatus, a planar geometry is assumed. A further simplification is made by assuming that heat transfer through the planar system is one-dimensional.

Heat transfer upon and within the material layers of the garment involves the processes of conduction, convection, and thermal radiation. The relevance of each of these processes depends on local conditions. For example, convective heat transfer is assumed to occur only on the outside boundaries of the clothing ensemble, so it enters through the boundary conditions of the model. In one dimension, the equation governing the conservation of energy is:

$$\rho c_p \frac{\partial T}{\partial t} = -\frac{\partial q_{CD}}{\partial x} - \frac{\partial q_R}{\partial x} + g, \quad (3.1)$$

with fluxes

$$q_{CD} = -k \frac{\partial T}{\partial x}, \quad \text{conduction (Fourier law),} \quad (3.2)$$

$$q_R, \quad \text{radiation flux (see Sec. 3.1).} \quad (3.3)$$

Equation 3.1 is solved in each gas or solid region of the garment. An initial condition and boundary conditions are both required. Care must be taken in the discretization of Equation 3.1 to ensure that the fluxes are continuous across interfaces (see the section on turnout coat characteristics). To obtain the temperature distribution throughout the protective clothing ensemble, both the energy Equation 3.1 and the radiative heat transfer equation, in some approximation, must be solved. The thermal radiation model is developed next.

3.1 Thermal Radiation Model

The radiative transfer equation for the spectral intensity, I_λ , in the absence of scattering and assuming thermodynamic equilibrium (Kirchoff's law is valid) is

$$\frac{1}{\kappa_\lambda} \frac{dI_\lambda(s, \theta, \phi)}{ds} + I_\lambda(s, \theta, \phi) = I_{b,\lambda}[T(s)], \quad (3.4)$$

where s is the path length of the radiation beam in the $\hat{\Omega}$ direction; θ and ϕ are the polar and azimuthal angles locating the beam of radiation in a spherical coordinate system; $I_{b,\lambda}$ is the blackbody spectral intensity; and T is the temperature. In general, s depends on three space variables. In the context of the one-dimensional model used here (see Figure 6), the intensity is independent of the azimuthal direction and points in the $\theta = 0$ or π directions (forward or backward) only. Thus, $\theta = 0$ corresponds to the direction of increasing x and

$$\frac{d}{ds} = \frac{\partial}{\partial x} \frac{dx}{ds} = \beta \frac{\partial}{\partial x}, \quad \frac{d}{ds} = \frac{\partial}{\partial x} \frac{dx}{ds} = \beta \frac{\partial}{\partial x}, \quad (3.5)$$

This motivates the splitting of the intensity into forward—positive x direction—and backward components, I and I^* :

$$I_\lambda = I_\lambda(x, \hat{\Omega}) = I_\lambda^+(x, \hat{\Omega}) + I_\lambda^-(x, \hat{\Omega}) = I_\lambda^+(x)\delta(\beta - 1) + I_\lambda^-(x)\delta(1 + \beta) \quad (3.6)$$

When variables are spectrally dependent, the λ subscript is present only on the left side of the equations to follow. Equation 3.4 is solved for a material layer—air layers are assumed to be nonparticipating—for both the backward and forward components of the spectral intensity. Figure 7 depicts this scenario for an arbitrary material layer l .

The solution of Equation 3.4 is

$$I_\lambda^+(x) = I^{i,+} e^{-\eta} + \int_0^\eta I_b e^{-(\eta-\eta')} d\eta',$$

$$I_\lambda^-(x) = I^{i,-} e^{-(\eta_d-\eta)} + \int_\eta^{\eta_d} I_b e^{-(\eta'-\eta)} d\eta', \quad (3.7)$$

where

$$\eta_\lambda = \int_0^x \kappa dx', \quad (3.8)$$

is the nondimensional spectral absorption length. From the spectral intensities in Equation 3.7, the spectral radiative flux can be determined.

$$q_{R,\lambda} = \int_{4\pi} \Omega I(s, \hat{\Omega}) d\Omega = q_{R,\lambda}^+ + q_{R,\lambda}^-$$

$$= \int_0^{2\pi} \int_0^1 I^+(x, \beta) \beta d\beta d\phi + \int_0^{2\pi} \int_{-1}^0 I^-(x, \beta) \beta d\beta d\phi. \quad (3.9)$$

Only the net flux, which is found by integrating Equation 3.7 over all wavelengths, is considered in the model

$$q_R^+(\eta) = q_R^{i+} e^{-\eta} + \sigma \int_0^\eta T^4(\eta') e^{-(\eta-\eta')} d\eta',$$

$$q_R^-(\eta) = q_R^{i-} e^{-(\eta_d-\eta)} - \sigma \int_\eta^{\eta_d} T^4(\eta') e^{-(\eta'-\eta)} d\eta', \quad (3.10)$$

where, $q_R^{i-} \leq 0$, the backward flux incident on the $x=d$ material boundary is non-positive. Note that spectral dependence of the fluxes can be added to the model in a straightforward way. The first terms on the right side of Equation 3.10 are the contribution to the flux of radiation entering the boundaries. The second terms are the contribution of emission along the path length of integration, or self emission.

In the current model, the major radiative fluxes incident on the boundaries of a material layer (q_R^{i+}, q_R^{i-}) are assumed to be due to:

1. The external incident heat flux on the outer garment layer, which contributes to the forward incident fluxes and the backward incident fluxes on the

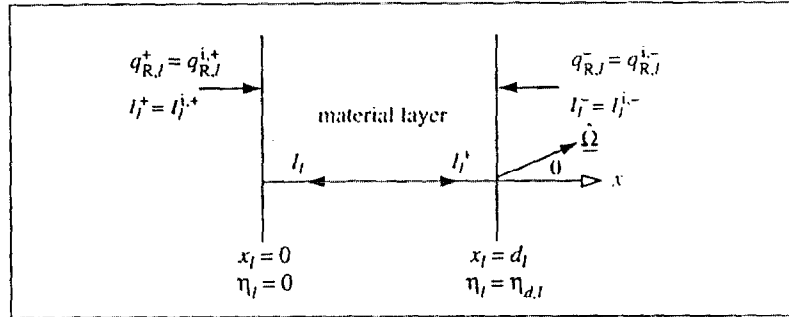


Figure 7.

inner gas/solid boundaries if reflection occurs.

2. Interlayer—that is, across air layers—radiative flux and its reflection. This occurs when the material surfaces that surround the air layers have different temperatures, and it contributes to both the forward and backward incident flux.

Only the backward reflection of radiation due to the external flux is calculated in Number 1. Since the radiative transfer equation is linear, the separate contributions to the forward or backward boundary fluxes for a particular boundary can be obtained and then added.

It is commonly assumed that, within a material, the contribution to the radiative flux from self emission is much smaller than that due to the absorption of the externally flux. For example, terms containing I_b in Equation 3.7 are neglected. Under this assumption, the net flux within material layer l from Equations 3.9 and 3.10 is (Beer-Lambert law)

$$q_{R,l} = q_{R,l}^+ + q_{R,l}^- = q_{R,l}^{i+} e^{-\eta_l} + q_{R,l}^{i-} e^{\eta_l - \eta_{d,l}}. \quad (3.11)$$

Here, $q_{R,l}^+$ and $q_{R,l}^-$ are the fluxes on the left and right side, respectively, of material layer l and are the optical length from the left boundary of layer l (see Figure 7).

The absorptivity of a fabric layer, α , is related to its transmissivity, τ , and reflectivity, r , through

$$\alpha + r + \tau = 1. \quad (3.12)$$

The absorption coefficient is assumed to be constant within a material layer, which means that it can be determined from the transmissivity and reflectivity of the fabric layer. Define q_{in} to be the radiative flux on the left surface of fabric layer l . From Equation 3.11, the transmissivity of the fabric layer is

$$\tau_l = \frac{q_{R,l}^+(\eta_{d,l})}{q_{in}} = \frac{(1 - r_l) q_{in} e^{-\kappa_l d_l}}{q_{in}}. \quad (3.13)$$

This equation gives the absorption coefficient for material layer l

$$\kappa_l = \frac{1}{d_l} \ln \left(\frac{1 - r_l}{\tau_l} \right). \quad (3.14)$$

3.2 Radiation fluxes on material boundaries

As discussed, it is assumed that the radiant flux on a material boundary comes from two sources: the external radiation source, q_e , and the interlayer flux, denot-

ed, for example, as q_{1-2} for fabric layers 1 and 2. These fluxes are depicted in Figure 8. The contributions to the incident boundary flux due to the external flux, q_e^{i+} , are as follows. Note, the backward component is due to reflection only from the next material layer.

Fabric Layer 1

$$q_{e,1}^{i+} = q_e(1 - r_1)$$

$$q_{e,1}^{i-} = -r_2 q_{R,1}^+ (\eta_{d,1}) = -q_e r_2 (1 - r_1) e^{-\eta_{d,1}} \quad (3.15)$$

Fabric Layer 2

$$q_{e,2}^{i+} = (1 - r_2) q_{R,1}^+ (\eta_{d,1}) = q_e (1 - r_2) (1 - r_1) e^{-\eta_{d,1}}$$

$$q_{e,2}^{i-} = -r_3 q_{R,2}^+ (\eta_{d,2}) = -q_e r_3 (1 - r_2) (1 - r_1) e^{-(\eta_{d,1} + \eta_{d,2})} \quad (3.16)$$

Fabric Layer 3

$$q_{e,3}^{i+} = (1 - r_3) q_{R,2}^+ (\eta_{d,2}) = q_e (1 - r_3) (1 - r_2) (1 - r_1) e^{-(\eta_{d,1} + \eta_{d,2})}$$

$$q_{e,3}^{i-} = 0 \quad (3.17)$$

Note that all boundary fluxes are in terms of the radiative properties of the material layers and the external flux.

Compute the net interlayer radiative flux by using the result for plane parallel plates with isotropic scattering, diffusively reflecting boundaries separated by

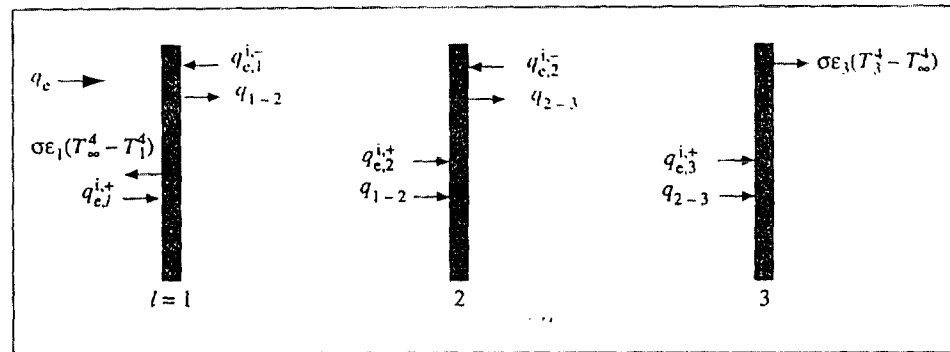


Figure 8.

nonparticipating air (optically thin, $\kappa_a d_a \ll 1$). With this assumption, q_{1-2} from Equation 3.9 for intensities integrated over all wavelengths¹⁶ is

$$q_{1-2} = \frac{\sigma(\epsilon_1 T_1^4 + r_1 \epsilon_2 T_2^4)}{1 - r_1 r_2} - \frac{\sigma(\epsilon_2 T_2^4 + r_2 \epsilon_1 T_1^4)}{1 - r_1 r_2} \quad (3.18)$$

Thus, the net incident flux on the left side of material layer $l=2$, for example, is the sum of the two contributions

$$q_{R,2}^{i,*} = q_{c,2}^{i,*} + q_{1-2} \quad (3.19)$$

This incident flux is used in Equation 3.11.

4 Numerical model

A control volume approach was used to derive the finite difference form of Equation 3.1. This method of discretization ensures local energy conservation and requires approximation of only first-order derivatives, rather than higher order. A second-order Runge-Kutta scheme was used for time stepping. The stability characteristics of Runge-Kutta are not as attractive as an implicit scheme such as Crank–Nicholson, leading to a more computationally expensive algorithm. However, the Runge-Kutta scheme was chosen at this stage of the model's development because it allows for a more simple and direct incorporation of a temperature-dependent conductivity.

4.1 Discretization of model equation

Material interfaces occur at control volume interfaces. An arbitrary control volume surrounding grid point P at the center of the control volume is depicted in Figure 9.

Control volume faces are marked by dashed lines; the left face is denoted by w and the right by e . Grid points to the left and right of P are denoted by W and E , respectively. Note that in general the control volumes are not of constant size—that is, $\delta_x \neq \delta_x, \Delta x = (\delta_x + \delta_x)/2$. Integrating Equation 3.1 over the control volume centered about P gives

$$\int_w^e c_p \rho \frac{\partial T}{\partial t} dx dA = k \left. \frac{\partial T}{\partial x} \right|_w^e dA - q_R \Big|_w^e dA + \int_w^e g dx dA, \quad (4.1)$$

where dA is a constant and the conductivity k can depend on temperature. Note that the equation is nonlinear when the conductivity k depends on temperature. The approach for each term in Equation 4.1 is discussed briefly below.

1. It is assumed that the rate at which energy is stored in the control volume, $c_p \rho \frac{\partial T}{\partial t}$, is constant throughout the volume. The validity of this assumption will improve as the size of the control volume decreases.

2. The first-order derivatives in the conduction flux term are obtained by

assuming T varies linearly within a control volume. Take care to ensure that the flux $-q_{co} = k\partial T/\partial x$ is continuous at cell interfaces. This is achieved by determining an effective conductivity coefficient, k^* , at the cell interface as follows. The heat conduction flux at interface e in Figure 9 is expressed as

$$k \frac{\partial T}{\partial x} \Big|_e = k_E \frac{(T_E - T_e)}{\delta_e^+} = k_P \frac{(T_e - T_P)}{\delta_e^-} \quad (4.2)$$

Note that the conductivity is assumed to be constant within a control volume. Solving for T_e from the second and third terms and substituting the result into the second term gives

$$k \frac{\partial T}{\partial x} \Big|_e = k^*(T_E - T_P), \quad 1/k^* = \frac{\delta_e^-}{k_P} + \frac{\delta_e^+}{k_E} \quad (4.3)$$

A similar method is used for fluxes at the gas/solid boundaries.

3. The radiative flux is obtained from Equation 3.11.

4. Internal heat generation may occur if, for example, a melting fabric solidifies, and heat losses may occur when the fabric pyrolyzes or melts. These processes are not considered at this stage of the model ($s=0$).

With the above assumptions, the discretized energy equation becomes

$$\overline{c_p \rho} \frac{\partial T}{\partial t} \Big|_p \Delta x dA = k \frac{\partial T}{\partial x} \Big|_w dA - q_R \Big|_w dA \quad (4.4)$$

where the overbar indicates the quantity is a cell average. This equation is solved for each material layer and air gap. Boundary conditions for the conductive and radiation fluxes are needed on all internal gas/solid boundaries. Convective losses must also be included at the two outer gas/solid boundaries. These boundary fluxes are considered next.

4.2 Boundary conditions

The external radiative flux, which is possibly time-varying, on the outer surface of the garment is specified, as are the ambient air temperatures on each side of

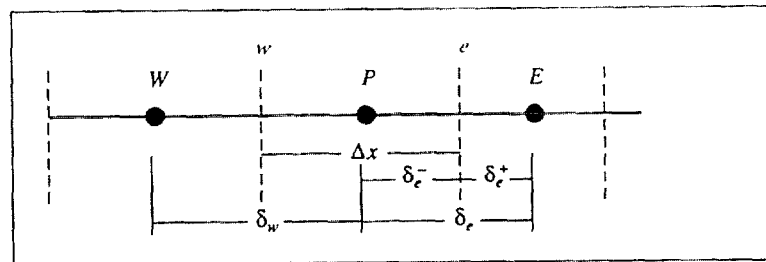


Figure 9.

the fabric assembly. Continuity of the heat fluxes across the gas/solid boundaries must be enforced to conserve energy. There are two types of gas/solid boundaries distinguished by the presence or absence of convective heat transfer. The two outer boundaries of a garment involve convective heat transfer and the associated surface heat transfer coefficient, h_c (see Figure 6). The thickness of the air gaps between fabric layers (~ 1 mm) is small enough to assume that no velocity boundary layer develops and heat transfer is by conduction.

Figure 10 depicts the situation for the outer surface of the garment facing the external radiation source. The solid and gas cells have mean temperatures T_s and T_g . The temperatures on the solid and gas sides of the surface layer are T_r and T_g , respectively. Continuity of the fluxes across the surface layer requires (using the cell spacing of Figure 9)

$$-q(x_r) = \frac{k_s}{\delta_e^+} (T_s - T_r) = h_c (T_r - T_g) = \frac{k_g}{\delta_e^-} (T_g - T_g). \quad (4.5)$$

Solving for the surface layer temperatures T_r and T_g and substituting the result into Equation 4.5 gives

$$-q(x_r) = k_r (T_s - T_g), \quad \frac{1}{k_r} = \frac{\delta_e^-}{k_s} + \frac{\delta_e^+}{k_g} + \frac{1}{h_c}. \quad (4.6)$$

The surface heat transfer coefficient, h_c , was obtained from the Nusselt number through empirical correlations of free convection on a vertical plate.¹⁷

$$h_c = \text{Nu} \frac{k_g}{L}. \quad (4.7)$$

Correlations appropriate for both laminar and turbulent flow were used, depending on the magnitude of the Rayleigh number. For laminar flow, the correlation is

$$\text{Nu} = 0.68 + \frac{0.67 \text{Ra}^{1/4}}{\left(1 + [0.492/\text{Pr}]^{9/16}\right)^{4/9}}, \quad 10^{-1} < \text{Ra} < 10^9. \quad (4.8)$$

When $\text{Ra} > 10^9$, the following correlation for turbulent flow was used

$$\text{Nu}^{1/2} = 0.825 + \frac{0.387 \text{Ra}^{1/4}}{\left(1 + [0.492/\text{Pr}]^{9/16}\right)^{8/27}}. \quad (4.9)$$

The temperature-dependent values of density and viscosity of air used in the Nusselt number were determined at $T_c + T_c/2$. A constant value of the Prandtl number was used, $\text{Pr} = 0.7$. Equation 4.6 defined the conductive heat flux in Equation 4.4 at the outer boundaries. Radiative fluxes on the boundaries were obtained from expressions developed in Section 3.2.

Similarly, at the gas/solid boundaries of the internal material layer 2, for which

no thermal boundary layer exists, continuity of the conductive heat fluxes across the interface is ensured by using

$$-q(x_r) = k_r(T_s - T_G), \quad \frac{1}{k_r} = \frac{\delta_e^-}{k_s} + \frac{\delta_e^+}{k_G} \quad (4.10)$$

5 Turnout Coat Characteristics

As depicted in Figure 6, a typical turnout coat consists of three fabric layers: the shell, which is the outermost layer, farthest from skin; the moisture barrier; and the thermal liner. Table 1 lists various physical characteristics of the fabrics under normal loft. To perform a simulation, the thickness, density, conductivity, specific heat, and optical properties of transmissivity and reflectivity were needed for each fabric layer. All the fabrics were clean and unused. Thickness was measured with a micrometer. For a given fabric, three different samples were measured 12 times, giving a total of 36 independent measurements. When possible, density was obtained in two ways: from the measured thickness, area, and mass and from the measured thickness and area density from the manufacturer. In the turnout coat considered here, the shell material is Nomex[®] IIIA, the moisture barrier is neoprene, and the thermal liner is Aralite[®].

The conductivity, specific heat, and optical properties of the fabrics were not measured. When possible, these property values were obtained from the literature; references are cited in Table 1. When no values could be found, those for similar fabrics were used until measured values could be obtained. For example, the specific heats of soft rubber and glass wool were used for the moisture barrier and thermal layer, respectively. Table 1 lists the material properties used in the simulations reported here.

As mentioned, the model used the total or spectrally integrated value of the transmissivity and reflectivity, which were calculated from their spectrally dependent values. In the case of the shell layer, for example,

TABLE 1
Physical characteristics of fabric layers (at 20°C)

Fabric Characteristic	Shell	Moisture Barrier	Thermal Liner
Thickness (cm)	0.082±0.007	0.055±0.005	0.35±0.04
specific mass (g/m ²)	254	440	240
density (g/cm ³)	0.31±0.024	0.8±0.06	0.072±0.007
conductivity (W/cm·C)	4.7x10 ⁻⁴ [1]	1.2x10 ⁻⁴ (soft rubber, [17])	3.8x10 ⁻⁴ (glass wool, [17])
specific heat (J/g·C)	1.3 [1]	2.01 (soft rubber, [17])	0.7 (glass wool, [17])
transmissivity (see text)	0.044	0.005	0.0012
reflectivity (see text)	0.09	0.017	0.002
color	black	white	yellow

$$\tau_1 = \frac{\int_0^\infty E_{b,\lambda} \tau_{\lambda,1} d\lambda}{\int_0^\infty E_{b,\lambda} d\lambda}, \quad r_1 = \frac{\int_0^\infty E_{b,\lambda} r_{\lambda,1} d\lambda}{\int_0^\infty E_{b,\lambda} d\lambda} \quad (5.1)$$

The spectral energy distribution from the central region of a gas-fired radiant panel approximates that of a black body source at 943 K¹⁸, which was used for $E_{b,\lambda}$ in Equation 5.1.

Bamford and Boydell¹⁹ use the specific mass of the fabric to determine values of τ_λ and r_λ for four wave length bands (visible, 0.4 μm to 0.7 μm ; 0.7 μm to 2.5 μm ; 2.5 μm to 5 μm ; and more than 5 μm). These band-averaged transmissivities can then be used in Equation 5.1. Note that the method used by Bamford and Boydell¹⁹ to obtain τ and r is based on a compilation of optical property measurements.⁴

Common clothing fabrics, such as cotton, polyester, acetate, acrylic, and wool, were measured. More specialized fabrics used in firefighter protective clothing, such as Nomex[®], were not considered. Thus, the accuracy of the optical properties obtained using Bamford and Boydell should be viewed with some caution. For example, Figure 6 in Quintiere¹⁹ shows that twill cottons and aromatic polyamide, which is the generic term for Nomex[®], of the same specific mass have markedly different spectral behavior in the wavelength range of 0.7 μm to 2.5 μm .

Even when the total transmissivity for a given fabric is measured, different values are reported. For a shell fabric with a specific mass of approximately 140 g/m², reported values are $\tau = 0.11$ for aromatic polyamide with a 1,000 K black body source;¹⁹ $\tau = 0.17$ for Nomex with a 1,250 K blackbody source.⁵ The method used by Bamford and Boydell gives $\tau = 0.08$ with a 1,100 K black body source. Similarly, the total reflectivities for the cases just considered are $r =$

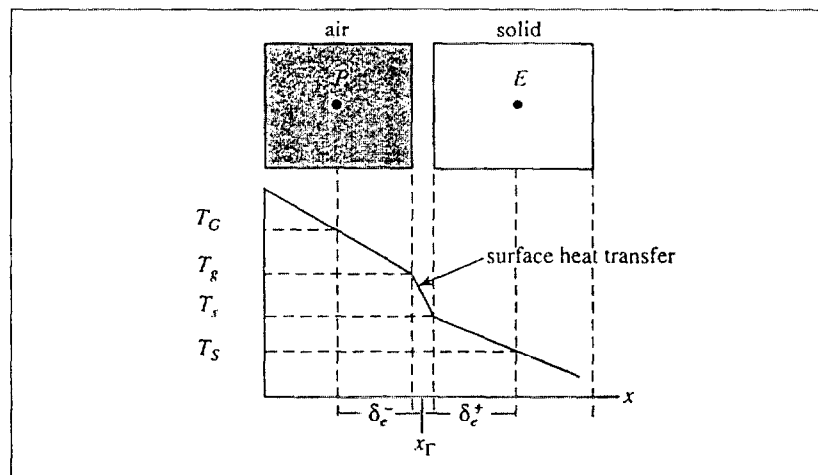


Figure 10.

0.24,¹⁹ $r = 0.26$,⁵ and $r = 0.09$ from Bamford and Boydell. As with the transmissivity, the reflectivity of Nomex* obtained following Bamford and Boydell is lower than those in the literature. In fact, Quintiere found that, regardless of color or specific mass, $r = 0.22$ for a number of commonly used cotton-based and aromatic polyamide shell fabrics with a 1,000 K black body source temperature.

It is clear from the variation of the optical property values in the literature that these properties need to be measured for the specific fabric to be simulated. Pending these measurements, however, base case values of the spectral transmissivity and reflectivity for each fabric layer were determined using Bamford and Boydell's method. This was done because no optical property information was found on neoprene or Aralite*, and Bamford and Boydell's method only requires the specific mass. Figure 11 shows the normalized spectral black body emissive power and spectral transmissivity from which the total transmissivity was calculated) for the Nomex* IIIA shell fabric used in this study (see Equation 5.2). The total reflectivity of the shell was computed in a similar manner. The moisture barrier was subjected to the gas-fired panel's radiative spectrum as transmitted in modified form through the shell. From the definition of the spectral transmissivity,¹⁷ the spectral emissive power on the moisture barrier is

$$E_{\lambda,2} = \tau_{\lambda,1} E_{b,\lambda} . \quad (5.2)$$

Equation 5.2 and the spectral transmissivity of the moisture barrier were used in Equation 5.1 to compute the total transmissivity of the moisture barrier. The total reflectivity of the moisture barrier was computed in a similar manner. Table 1 gives the base case values of the optical properties. Both air gaps were assumed

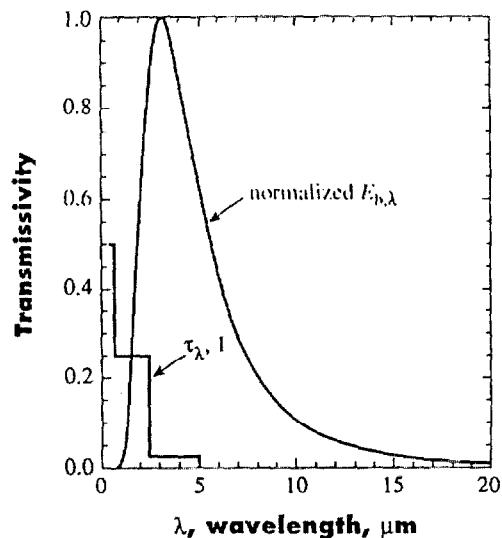


Figure 11.

to be 1 mm thick.

The specific heat of air, which is weakly dependent on temperature, was set equal to its value at 20°C (1.006 J/g·C). The temperature dependence of the conductivity and density of air were fitted by polynomials. Using temperature-dependent density and viscosity for air influenced the simulation results mainly by changing the Nusselt number. That is, simulation results with variable properties for the air layers were significantly different from results with constant air properties—difference of 5°C—only if the variable properties were used in the Nusselt number. Preliminary sensitivity tests suggested that using variable thermal properties for the fabric layers will not have a significant effect on simulation results over the range of conditions considered here. This issue needs further investigation with accurately measured, temperature-dependent thermal properties of the fabrics.

6 Model Results

6.1 Verification

It is useful to compare the results of the numerical method to exact solutions of simplified problems. The performance of the numerical method can then be tested, and the grid resolution required for suitably accurate results can be determined. To test the model for the case of two materials with different properties, the exact solution to the following problem was used:

$$U(x, t) = T(x, t) - T(x, 0),$$

$$\frac{\partial U_1}{\partial t} = D_1 \frac{\partial^2 U_1}{\partial x^2}, \quad 0 \leq x \leq x_r; \quad \frac{\partial U_2}{\partial t} = D_2 \frac{\partial^2 U_2}{\partial x^2}, \quad x_r \leq x$$

$$\frac{\partial U_1}{\partial t} = D_1 \frac{\partial^2 U_1}{\partial x^2}, \quad 0 \leq x \leq x_r; \quad \frac{\partial U_2}{\partial t} = D_2 \frac{\partial^2 U_2}{\partial x^2}, \quad x_r \leq x \quad (6.1)$$

Equation 6.1, along with continuity conditions of both U and its flux at the interface two different materials ($x = x_r$), governs the change in temperature due to a constant flux H on the $x = 0$ boundary. The solution has been found using Laplace transforms²⁰ with corrections.⁶ The prescribed constant boundary flux H can be viewed as the net flux due to radiation, conduction, and convection at the boundary. Time-dependent radiative and convective heat losses at the boundary, which increase with temperature, are not present. The exact solution to Equation 6.1 is

$$-\frac{1}{\gamma} \sum_{n=0}^{\infty} \left(\frac{1}{\gamma}\right)^n \left[2 \sqrt{\frac{D_1 t}{\pi}} \left(e^{-\frac{a^2}{4D_1 t}} + e^{-\frac{b^2}{4D_1 t}} \right) - a \left\{ 1 - \operatorname{erf} \left(\frac{a}{2\sqrt{D_1 t}} \right) \right\} \right]$$

$$-\frac{1}{\gamma} \sum_{n=0}^{\infty} \left(\frac{1}{\gamma}\right)^n \left[2\sqrt{\frac{D_1 t}{\pi}} \left(e^{-\frac{a^2}{4D_1 t}} + e^{-\frac{b^2}{4D_1 t}} \right) - a \left\{ 1 - \operatorname{erf} \left(\frac{a}{2\sqrt{D_1 t}} \right) \right\} + b \left\{ 1 - \operatorname{erf} \left(\frac{b}{2\sqrt{D_1 t}} \right) \right\} \right] \quad (6.2)$$

$$U_2 = \frac{2H\alpha\sqrt{D_1}}{x_r} \sum_{n=0}^{\infty} \left(-\frac{1}{\gamma}\right)^n \left\{ 2\sqrt{\frac{D_2 t}{\pi}} e^{-\frac{c^2}{4D_2 t}} - c \left(1 - \operatorname{erf} \frac{c}{2\sqrt{D_2 t}} \right) \right\} \quad (6.3)$$

and at the material interface, ($x = x_r$),

$$U(x_r, t) = \frac{H}{k_1} \sum_{n=0}^{\infty} \left(-\frac{1}{\gamma}\right)^n \left(1 - \frac{1}{\gamma}\right) \left[2\sqrt{\frac{D_1 t}{\pi}} e^{-\left(\frac{x_r(2n+1)}{2\sqrt{D_1 t}}\right)^2} - x_r(2n+1) \left(1 - \operatorname{erf} \frac{x_r(2n+1)}{2\sqrt{D_1 t}} \right) \right] \quad (6.4)$$

where

$$\gamma = \frac{k_2 c_{p,2} \rho_2 + \sqrt{k_1 c_{p,1} \rho_1 k_2 c_{p,2} \rho_2}}{k_2 c_{p,2} \rho_2 - \sqrt{k_1 c_{p,1} \rho_1 k_2 c_{p,2} \rho_2}},$$

$$\alpha = (k_2 \sqrt{D_1} - k_1 \sqrt{D_2})^{-1},$$

$$a = x + 2x_r(n+1),$$

$$b = x - 2x_r(n+1),$$

$$c = x - x_r \left\{ 1 - \sqrt{D_2/D_1} (2n+1) \right\}.$$

This solution can be used to ensure that the discontinuity of the conduction coefficient at the material interface is handled properly by the numerical method. Unlike the flux due to conduction, the radiative flux in Equation 4.4 was direct-

ly modeled. Its accuracy depends on the validity of the physical model for radiative heat transfer and on using appropriate optical properties, not on the accuracy of numerical differentiation. Thus, even though radiative absorption and emission are absent, using Equation 6.1 does test the accuracy of the full numerical model. A minor exception to this statement will be discussed.

The case of a $x_r = 0.5$ mm layer of Nomex[®] against a 5 mm layer of neoprene was simulated. The external flux was 0.25 W/cm^2 . This flux was also used in the simulation of an experimental test apparatus case discussed below. Material properties from Table 1 were used. The temperature profile throughout the two material layers at $t = 60$ s is shown in Figure 12(a). Temperatures from the exact solution at computational grid point, are shown as dots.

The Nomex[®]/neoprene interface can be seen to reside midway between the adjacent control volumes. Temperatures from the exact and numerical solutions are in excellent agreement. The temperature time histories at three locations in the fabric assembly are plotted in Figure 12(b). The exact and numerical temperatures are again in excellent agreement at the interior point $x = 1.5$ mm. Since numerical values of the temperature exist only at control volume centers, they are not known at material interfaces. This is the source of the disagreement ($|T_{\text{num},i} - T_{\text{exact},i}| \leq 3^\circ\text{C}$ at $t = 60\text{s}$) between the numerical and exact temperatures at $x = 0$ mm and $x = x_r = 0.5\text{mm}$ in Figure 12(b). Some error will therefore be introduced when computing the interlayer radiative fluxes (Equation 3.18) and the radiative flux to the ambient surroundings. However, the difference between the exact and numerical solution is sufficiently small that this error will be negligible.

The results above show that the numerical procedure accurately computed heat transfer through the interface between two fabrics commonly used in turnout coats.

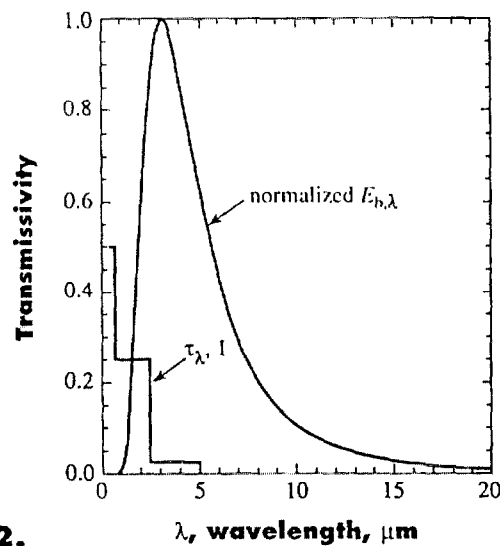


Figure 12.

λ , wavelength, μm

6.2 Turnout Coat Simulation

A turnout coat assembly with material characteristics listed in Table 1 was subjected to thermal radiation from a gas-fired radiation panel, as discussed in Section 2. The total radiative flux on the shell of the turnout coat was $q_c = 0.25$ W/cm². This flux is characteristic of the pre-flashover fire environment in which structural firefighters typically work.²²

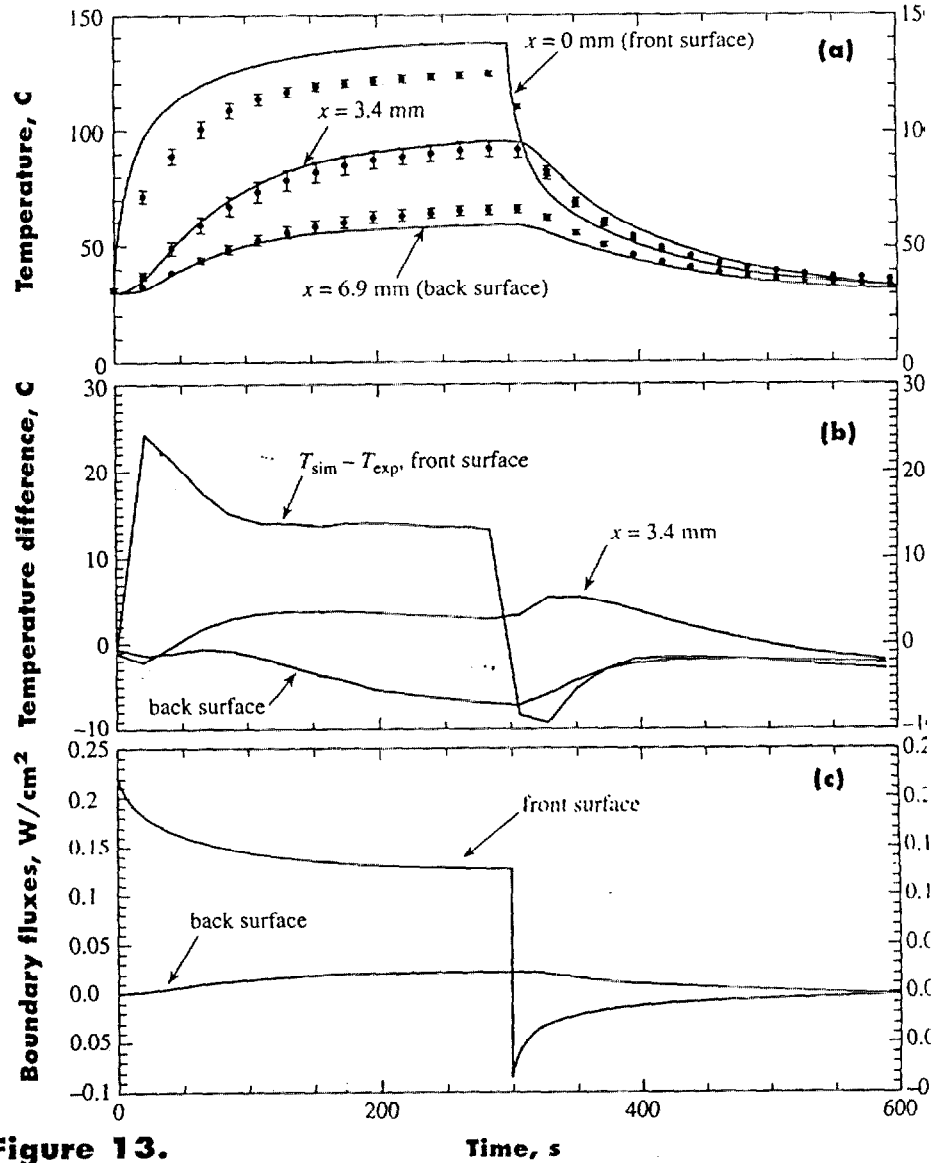


Figure 13.

Time, s

Thermocouples of type K and size 10 mil (0.254 mm) were sewn on the front surface of the shell ($x = 0$ mm) and on both the inner air/fabric interface ($x = 3.4$ mm) and the outer fabric/air interface ($x = 6.9$ mm, back surface of garment) of the thermal liner. The turnout coat material was subject to radiation from the gas panel for 300 seconds, after which a radiation shield was placed between the coat and the gas-fired panel. A cool-down period of approximately 10 minutes followed. The turnout coat sample was then removed from the experimental test apparatus. Ten such tests, separated by approximately 10 min, were completed. From these 10 tests, the mean and standard deviation of the temperature at each thermocouple were computed. The ambient mean temperature was found to be $T_a = 29.3^\circ\text{C}$.

Figure 13(a) plots the temperature time history from the simulation and experiment at the three thermocouple locations. The temperature difference between the simulation and the experiment (mean values) is plotted versus time in Figure 13(b). Heat transfer through the turnout coat reaches a steady state after approximately 100 seconds. Figure 14 shows the simulated and experimental temperatures versus distance into the turnout coat at three different times, $t = 0$ seconds, 200 seconds (during steady state), and 400 seconds. Vertical dotted lines mark the air/solid interfaces. Mean temperatures from the thermocouples (at $x = 0$ mm, $x = 3.4$ mm, and 6.9 mm) are plotted as black circles, with error bars extending one standard deviation above and below. Simulated temperatures are plotted as solid lines.

During the steady-state period, the simulated shell temperature is approximately 15°C higher than experimentally obtained temperatures. The largest error in the model occurred in the prediction of temperatures on the outer shell surface during the first half of the experiment before the flux from the radiant panel was blocked. A probable source of this error is the approximate manner in which the transmissivity and reflectivity values were obtained. A majority of the incident

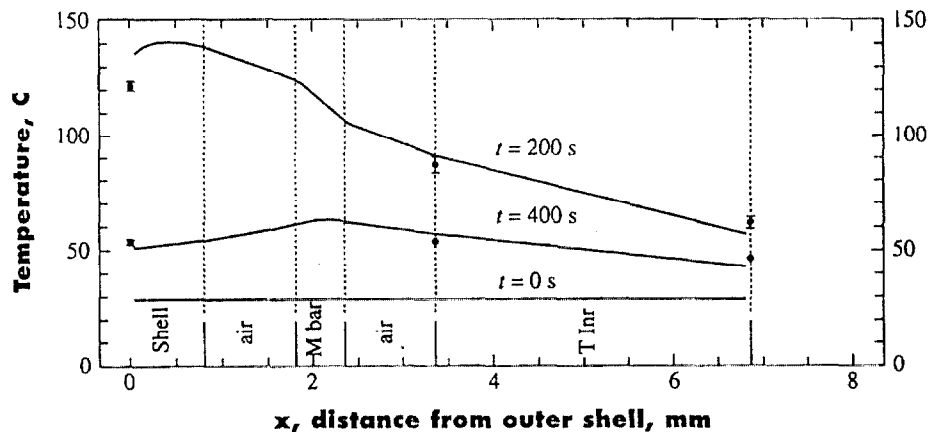


Figure 14.

radiant heat flux is absorbed by the shell. After the radiant panel is blocked, the material properties of the fabric layers, such as conductivity, specific heat, and density, play a more important role, as does convective heat loss from the boundaries. Thus, it is especially important in the case of the shell to use accurate values for the transmissivity and reflectivity. Note that during the cool-down period, the simulated and experimental temperatures for the shell agree better. The simulated temperatures in the interior of the garment were within approximately 5°C of the mean experimental temperature.

Based on these results, it appears that the model could be used to predict the thermal performance of firefighters' protective clothing, at least under heat flux conditions consistent with the model assumptions. More data from experiments using materials for which the optical and thermal properties of the materials are known is required before the accuracy of the model can be conclusively measured. Material properties necessary to model the thermal behavior of fabrics and fabric assemblies common in firefighter gear are currently being measured.

The net radiative flux from the simulation at both the front surface of the shell and the back surface of the thermal liner are plotted versus time in Figure 13(c). During the time interval $t = 0$ s to 300 seconds, the flux on the front surface was reduced from 0.25 W/cm² to 0.14 W/cm² by reflection and radiation to the surroundings. After radiation from the gas-fired panel was removed at 300 seconds, radiative cooling occurred. Note that if the ambient temperature is increased to 65°C, which is commonly experienced by firefighters,²² the net radiative flux on the shell at 300 seconds would increase to 0.16 W/cm² for the same shell temperature. On the back surface, the radiative flux gradually increased to a maximum of 0.025 W/cm² as the temperature of the thermal liner rose [see Figure 13(a)]. This flux was entirely due to the temperature of the thermal liner relative to the ambient temperature, T_{∞} , since the contribution of the external flux q_{∞} was negligible. If the ambient temperature is increased to $T_{\infty} = 32^{\circ}\text{C}$, which is normal core skin temperature, the back surface flux decreases to 0.023 W/cm² for the same thermal liner temperature.

Figures 13 through 14 show that the clothing ensemble clearly provided protection against the incident radiative flux. From the outside of the shell to the back of the thermal liner, the temperature fell nearly 70°C. The effects of the moisture barrier's lower thermal conductivity are apparent by the relatively steep drop in temperature in the $t = 200$ seconds temperature profile in Figure 14. The steady-state temperature at the back of the thermal liner reached 66°C. Note that when a firefighter wears a turnout coat, the apparent temperature in the air gap between the turnout coat and the firefighter will rise due to an increased relative humidity. For the incident flux and protective clothing assembly considered here, heat transfer to the firefighter would occur predominantly through conduction rather than radiation from the thermal liner.

7 Summary and Conclusions

The goal of this NIST project is to improve firefighter safety through better understanding of heat transfer in the protective garments they wear. Both experimental and modeling approaches were used. This paper focuses on the formulation of the first stage in a heat transfer model suitable for predicting temperature and heat flux in firefighter protective clothing. For this reason, model results were compared to only one experimental case ($q_r = 0.25 \text{ W/cm}^2$, typical of pre-flashover fires) with one commonly used three-layer protective clothing assembly. Model predictions of the temperature agreed very well with experimental temperature for the interior layers (within 5°C). Temperature predictions on the outer shell were up to 24°C higher than experimentally measured values while the external radiative flux was present. Error in the estimates of transmissivity and reflectivity was most likely the source of modeling error in the shell temperatures.

No measurements of these optical properties for any of the fabrics were available. Instead, these property values were based on previous work. NIST is currently developing a database of material properties for fabrics and materials common in firefighter protective gear. Further application and testing of the model using other fabric assemblies and heat flux environments is needed to verify the model.

The model was designed, as much as possible, to accommodate the variable thermal environments in which firefighters work. While this capability was not shown here, the incident radiative heat flux, fabric thickness, air gap thickness, and the presence or absence of an air gap can be varied dynamically during the simulation.

At this stage, the model is restricted to dry fabrics and to temperature and flux levels, which are low enough that no thermal degradation of the fabric occurs. Further developments should include moisture effects and a multiple-layer, variable-property skin mode. Estimations of burn injury risk would then be possible.

8 Acknowledgments

Appreciation is extended to Mr. Robert T. McCarthy of the United States Fire Administration for assistance provided during discussions of firefighter burn injuries and protective clothing performance. The United States Fire Administration provided funding for the National Institute of Standards and Technology, Building and Fire Research Laboratory, to study issues related to firefighter's station/work uniforms and protective clothing. Mr. William Twilley of the Building and Fire Research Laboratory assisted in the development of the experimental test apparatus.

References

1. Torvi, D. A., "Heat Transfer in Thin Fibrous Materials Under High Heat Flux

Nomenclature

c_p	[J/K•kg] specific heat
d	[m] thickness of a material layer
d_a	[m] thickness of air layer
e	interface between control volumes P and E
D	(m ² /s) diffusivity ($k/\rho c_p$)
E	midpoint of right control volume in finite difference scheme
$E_{b,\lambda}$	[W/(m ² •μm)] spectral blackbody emissive power
$E_{\lambda,l}$	spectral emissive power incident on fabric layer l
g	[W/m ³] internal energy generation rate per unit volume or [m/s ²] gravitational acceleration
h_c	[W/m ² •K] surface heat transfer coefficient for convection
Gr	$= 2g(T - T_\infty)L^3/\nu^2$ (Grashof number)
I	[W/m ² •μm•sr] radiant intensity
$I_{b,\lambda}$	blackbody spectral intensity
k	[W/K•m] thermal conductivity
k^*	effective conductivity coefficient, used in determining q_{CD} at internal cell interfaces
k_r	effective conductivity coefficient, used in determining q_{CD} at gas/solid interfaces
L	[m] streamwise distance to the initiation of natural convection
Nu	Nusselt number
P	midpoint of central control volume in finite difference scheme
Pr	$= \mu c_p/k$ Prandtl number
q	[W/m ²] heat flux
q_{CD}	heat flux due to conduction
q_e	external radiation heat flux on left side of the first protective clothing layer (shell layer)
q_R	radiation heat flux
Ra	$= Pr[Gr]$, Rayleigh number
r	reflectivity of incident thermal radiation
s	[m] pathlength of radiation beam
t	[s] time
T	[K] temperature
T_∞	ambient air temperature
w	interface between control volumes W and P
W	midpoint of left control volume in finite difference scheme
x	[m] distance measure into protective clothing

Nomenclature, continued**Greek symbols**

α	absorptivity
β	$= \cos(\theta)$, cosine of polar angle locating radiation beam in spherical coordinates
δ	Dirac delta function
δ_e, δ_w	distance between midpoints of control volumes P and E , and P and W , respectively
δ_-	distance from cell interface e to point P in finite difference scheme
δ_+	distance from cell interface e to point E in finite difference scheme
ε	emissivity
η	nondimensional optical depth variable
θ	polar angle locating radiation beam in spherical coordinates
κ	[1/m] absorption (extinction) coefficient
λ	[μm] wavelength of thermal radiation
μ	[kg/(m \cdot s)] dynamic viscosity
ρ	[kg/m 3] mass density
σ	$5.6697 \times 10^{-8} \text{ W}/(\text{m}^2 \cdot \text{K}^4)$ Stefan-Boltzmann constant
τ	transmissivity of incident thermal radiation
ϕ	azimuthal angle locating radiation beam in spherical coordinates
$\hat{\Omega}$	direction of radiative energy propagation

Subscripts

1, 2...	material layers 1, 2, ...
a	air
d	total thickness of air gap or material layer
l	material or fabric layer l
G	gas cell
S	solid cell
Γ	gas/solid or solid/solid interface
λ	spectral dependence

Superscripts

+	forward direction
-	backward or reverse direction
i	incident (flux or intensity) on material boundary

- Conditions," Ph.D. thesis, Mechanical Eng. Dept., University of Alberta, Calgary, Alberta, 1997.
2. Chen, N.Y., "Transient Heat and Moisture Transfer Through Thermally Irradiated Cloth," Ph.D. thesis, Massachusetts Institute of Technology, Cambridge, Mass., 1959.
 3. Backer, S., et al., "Textile Fabric Flammability," The MIT Press, Cambridge, Mass., 1976.
 4. Wulff, W., Zuber, N., et al., "Study of Hazards from Burning Apparel and the Relation of Hazards to Test Methods," Second Final Report: Georgia Institute of Technology, NTIS: COM-73-10956, 1972.
 5. Morse, H. L., Green, K. A., Thompson, J. G., Moyer, C. B., and Clark, K. J., "Analysis of the Thermal Response of Protective Fabrics," Technical Report, Acurex Corp., Mountain View, Calif., 1972.
 6. Stoll, A. M., Chianta, M. A., and Munroe, L. R., "Flame-Contact Studies," *Transactions of the ASME, Journal of Heat Transfer*, Vol. 86, (1964), pp. 449—456.
 7. Stoll, A. M. and Chianta, M. A., "Burn Protection and Prevention in Convective and Radiant Heat Transfer," *Aerospace Medicine*, Vol. 39, 1968, pp. 1097—1100.
 8. Stoll, A.M. and Chianta, M.A. "Method and Rating System for Evaluation of Thermal Protection," *Aerospace Medicine*, Vol. 40, No. 11, pp. 1232 - 1238.
 9. American Society for Testing and Materials, ASTM D 4108-87, *Standard Test Method for Thermal Protective Performance of Materials for Clothing By Open-Flame Method*, West Conshohocken, Pa., 1987.
 10. Bamford, G. J. and Boydell, W., "ICARUS: A Code for Burn Injury Evaluation," *Fire Technology*, Vol. 31, No. 4 (1995), pp. 307—335.
 11. NFPA 1971, *Protective Ensemble for Structural Fire Fighting*, 1997 edition, National Fire Protection Association, Quincy, Mass.
 12. Krasny, J. F., Rockett, J. A., and Huang, D. "Protecting Fire Fighters Exposed in Foam Fires: Comparison of Results of Bench Scale Test for Thermal Protection and Conditions During Room Flashover," *Fire Technology*, Vol. 24, No. 1, (1988), pp. 5-19.
 13. Peacock, R.D., Krasny, J.F., Rockett, J.A. and Huang, D. "Protecting Fire Fighters Exposed in Room Fires, Part 2: Performance of Turnout Coat Materials Under Actual Fire Conditions," *Fire Technology*, Vol. 26, 1990, pp. 202—222.
 14. Lawson, J. R., "Fire Fighter's Protective Clothing and Thermal Environments of Structural Fire Fighting," *NISTIR 5804*, National Institute of Standards and Technology, Gaithersburg, Md., (1996).
 15. Lawson, J. R., "Development of an Apparatus for Measuring the Thermal Performance of Fire Fighter's Protective Clothing," *NISTIR 6400*, National Institute of Standards and Technology, Gaithersburg, Md., (1999).
 16. Özisik, M. N., *Radiative Transfer and Interactions with Conduction and*

Convection, John Wiley & Sons, New York, 1973.

17. Özisik, M. N., *Heat Transfer: A Basic Approach*, McGraw-Hill, Inc., New York, 1985.

18. Comeford, J. J., "The Spectral Distribution of Radiant Energy of a Gas-Fired Radiant Panel and Some Diffusion Flames," *Combustion and Flame*, Vol. 18, (1972), pp. 125—132.

19. Quintiere, J., "Radiative Characteristics of Fire Fighter's Coat Fabrics," *Fire Technology*, Vol 10, (1974), pp. 153—161.

20. Griffith, M. V. and Horton, G. K., "The Transient Flow of Heat Through a Two-Layer Wall," *Proceedings of the Philosophical Society*, London, England, Vol. 56 (1946), pp. 481—487.

21. Wu, Yung-Chi, "Material Properties Criteria for Thermal Safety," *Journal of Materials*, Vol. 4 (1972), pp. 573—579.

22. *Minimum Standards on Structural Fire Fighting Protective Clothing and Equipment: A Guide for Fire Service Education and Procurement*, Federal Emergency Management Agency, United States Fire Administration, FA-137, September 1993.